GA Based Pole Shape Optimization for Sound Noise Reduction in Switched Reluctance Motors

Ahmad Dadpour [1], and Kourosh Ansari [2]

[1]Ferdowsi University of Mashhad, a.dadpour@gu.ac.ir

[2]Ferdowsi University of Mashhad, k.ansari@um.ac.ir

Abstract: *In this paper an optimized pole shape is presented to reduce acoustic noise of switched reluctance motor (SRM). The optimization is based on the genetic algorithm and by considering both radial force and torque ripple reduction. A two-dimensional (2-D) finite element (FE) analysis is carried out to simulate the 6/4 SRM for each solution of the population generated by GA. To decrease the acoustic noise in SRM, arcs on the rotor and stator teeth are designed in three steps including: rotor with arcuate teeth, stator with arcuate teeth, and both stator and rotor with arcuate teeth. In the case of the stator with arcuate teeth, torque ripple and radial force decrease in comparison with the base motor while the average torque for this model is the same as the base motor. In the case of the rotor with arcuate teeth, torque ripple increases and radial force decreases. However, the radial force and torque ripple might be varied in the same or opposite direction. The best solution produced by the GA has been implemented on a real motor. Experimental results on a real motor demonstrate the validity of our proposed GA based optimized pole shape.*

1. Introduction

Switched reluctance motors (SRMs) develop torque through an interaction between the electromagnetic excitation from the stator poles and the rotor teeth. Once a particular combination of phase currents is established and maintained in the stator, the rotor teeth will be attracted into alignment with the stator poles in a particular position. This attraction force can be divided into tangential and radial force components relative to the rotor. The tangential force is converted into the rotational torque. It contains a significant radial force component in addition to the required tangential force [1].

The dominant source of the acoustic noise in the SRM has been shown to be the distortion of the stator by radial magnetic force. The other problem for SRMs is torque ripple which causes increased undesirable acoustic noise. It is also caused by the saliency of the stator and rotor [2].

Reviewing of literatures during recent years about acoustic noise reduction in SRM drive shows that some researchers worked on operating parameters of a switched reluctance drive. They changed some parameters such as the magnitude of phase currents and the time which these currents turned on or off. As a result of these changes, torque ripple was minimized [3, 4]. Some researchers minimized the radial force by changing of these parameters [5]. In several papers, the shapes of rotor and

stator poles were studied to decrease the torque ripple [6-10] or magnetic radial force [11].

All of the mentioned studies have done separately on either the torque ripple or radial magnetic force reduction. On the other hand, in these works torque ripple was decreased without any research on the radial force or counter. However, when torque ripple is decreased the radial force may be increased or decreased.

In this paper, the geometry of low magnetic radial force together with torque ripple is studied and a motor having optimized arcuate teeth is proposed. Its characteristics are simulated by finite element method (FEM) analysis and compared with SRMs having the conventional shape. Extensive two-dimensional (FE) analysis for a motor are required to determine the best stator and rotor pole arc values. Therefore, the optimum arcs of the stator and rotor pole of a SRM are obtained by using the genetic algorithm (GA).

A genetic algorithm was employed in [12] for optimizing the shape of magnets to minimize the cogging torque.

Applications of genetic optimization algorithm in estimation of the parameters of servo electrical drives and dynamic state of DC motor were proposed in [13] and [14], respectively. GA was used for optimization because of its power in searching whole solution space with more probability to finding the global optimum [13].

In [15] a speed controller design for a switched reluctance (SR) motor in order to achieve minimum torque ripple and high control performance was presented. Genetic algorithm optimized the turn-on and turn-off degrees of each phase, the parameters of PID controller in transient state, and parameters of PID controller that considered for reducing the torque ripple in steady state. Also, GA obtained the optimum parameters of three nonlinear gains considered for fuzzy switching between the two PID controllers.

In this paper the genetic algorithm is used to optimize the pole shape to reduce acoustic noise of switched reluctance motor (SRM). The rest of the paper is organized as follows: Dominant sources of the acoustic noise in SR motors are introduced in section 2. Simulation of the SR motor by using FE method is described in section 3. Three new SR motor designs are presented in

section 4. In section 5, the optimization of stator and rotor arcs by using the GA is described. Experimental system and conclusion are given in sections 6 and 7, respectively.

2. Magnetic Sources of Acoustic Noise

Radial force and torque ripple are the dominant sources of the acoustic noise in SRM. Each of these sources is carried out in this section.

a) Radial force

The magnetic flux in the SRM passes across the air gap in an approximate radial direction producing radial, tangential, and lateral forces on the stator and rotor. To determine the relationship between these forces and the SRM dimensions, the SRM is assumed to be operating in the linear region. Figure 1 illustrates the various dimensions involved in the derivation of these forces.
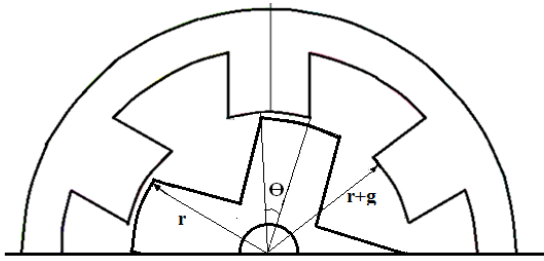

Fig. 1: Various dimensions of SRM

Consider that iron is infinitely permeable and has zero reluctance which leaves only the air gap to provide reluctance in the circuit. The air gap flux density at a given stator and rotor pole overlap angle (θ), air gap (l_g), and current (i) is given as $B_g(\theta,i,l_g)$. Let r be the outer radius of the rotor, L' be the stack length or iron length in the z direction, T_{ph} be the number of turns in one phase of the machine, H_g be the magnetic field strength, ϕ be the flux, and μ_0 be the permeability of air. Then the flux linkage is derived as:

$$\psi(\theta,i) = T_{ph}\phi = T_{ph}B_g A = T_{ph}\mu_0 H_g L'r\theta$$

$$= T_{ph}\mu_0 \frac{T_{ph}i}{l_g}L'r\theta = \mu_0 \frac{T_{ph}^2}{l_g}L'r\theta i \qquad (1)$$

The co-energy is given by:

$$W'(\theta,i) = \int \psi(\theta,i)di = \int \mu_0 \frac{T_{ph}^2}{l_g}L'r\theta i.di$$

$$= \mu_0 \frac{T_{ph}^2}{2l_g}L'r\theta i^2 \qquad (2)$$

It can be seen that the co-energy, $W'(\theta,i)$ is a state function of the four independent variable θ, i, l_g, and L'. Thus, its differential (radial force, lateral force and electromagnetic torque) can be expressed as:

$$F_r = \frac{\partial W'(\theta,i,l_g)}{\partial l_g} = \frac{\mu_0 L'r\theta T_{ph}^2}{2l_g^2}i^2 \qquad (3)$$

$$F_y = \frac{\partial W'(\theta,i,L')}{\partial L'} = \frac{\mu_0 r\theta T_{ph}^2}{2l_g}i^2 \qquad (4)$$

$$T = \frac{\partial W'(\theta,i)}{\partial \theta} = \frac{\mu_0 rL'T_{ph}^2}{2l_g}i^2 \qquad (5)$$

The tangential force is obtained by dividing the tangential torque by the radius of the rotor pole, yielding:

$$F_t = \frac{T}{r} = \frac{\mu_0 L'T_{ph}^2}{2l_g}i^2 \qquad (6)$$

The equations (3), (4), and (6) show that radial force is usually multiple times that of the tangential and lateral forces in the SRM. Such a large force causes stator vibrations. Moreover, the equations (3) and (5) show that radial force and torque are dependent on design parameters and square of phase current. Some of these parameters are common in two equations, and some like θ and l_g is able different effect on radial force and torque.

In addition to these parameters, the leakage flux, iron circuit reluctance, and saturation effect on radial force and torque. It is difficult to get the relation between these all phenomena and radial force and torque. So we should simulated the machine to see the effect of all these on the radial force and/or torque.

The inductance is obtained by dividing the flux linkage by the phase current, yielding:

$$L = \frac{\psi(\theta,i)}{i} = \mu_0 \frac{T_{ph}^2}{l_g}L'r\theta \qquad (7)$$

Then, substituting Eq. (7) in Eq. (5), the electromagnetic torque is obtained as:

$$T = \frac{1}{2}\frac{dL}{d\theta}i^2 \qquad (8)$$

b) Acoustic noise intensity

Sound power radiated by an electric machine can be expressed as [16]:

$$P = 4\sigma_{rel} \cdot \rho.c.\pi^2 \cdot f_{exc}^{~2} \cdot D_{circum}^{~~2} \cdot R_{out} \cdot L' \qquad (9)$$

Where c is the traveling speed of sound (m/s) in the medium, ρ is the density of air, R_{out} is the outer radius of the stator (m), L' is the stack length or iron length in the z direction, f_{exc} is the excitation frequencies (Hz) and σ_{rel} is the relative sound intensity and equal to:

$$\sigma_{rel} = \frac{k^2}{1+k^2}$$

Where k is the wave number and equal to:

$$k = \frac{2\pi \cdot R_{out} \cdot f_{exc}}{c}$$

Amplitude of dynamic deflection equal to:

$$D_{cicum} = \frac{\dfrac{12 F_{r_{per}}(f_{exc}) R_c}{m^4 E}(\dfrac{R_c}{h_s})^3}{\sqrt{(1-(\dfrac{f_{exc}}{f_m})^2)^2 + (\dfrac{\delta}{\pi}\dfrac{f_{exc}}{f_m})^2}} \qquad (10)$$

where $F_{r_{per}}$ is the Amplitude of radial force wave (N/m), δ is the logarithmic decrement and equal to $\delta = 2\pi\varsigma$

ς is the damping ratio and equal to:

$$\varsigma = \frac{c}{\sqrt{4KM}}$$

where K and M are the equivalent stiffness and mass.

$$f_{exc}(n) = n f_p = \frac{n\omega_m N_{rp}}{60} \qquad (11)$$

where N_{rp}, ω_m are the number of rotor poles and speed of the machine (r/min) and f_p is the fundamental frequency of phase current (Hz).

The equations (9) and (10) show that sound power radiated is proportional to the square amplitude of radial force. Therefore, to decrease the sound power radiated we must find a way to decrease the radial force.

c) Torque ripple

When motor is running and torque is not constant, we have torque ripple and noise. The expression for the torque ripple is [7]:

$$Torque\ Ripple = \frac{T_{max} - T_{min}}{T_{av}} \qquad (12)$$

where T_{max}, T_{min} are the maximal value and minimal value of total torque, T_{av} is the average value of total torque.

To noise reduction, we must decrease the torque ripple. The average torque is found out over that portion of the torque profile, which is actually utilized in the motor. In a 6/4 SRM, one phase will be excited for 30° or may be a little bit more. The authors would like to select that 30° where the torque is nearly constant. This choice will ensure maximum average torque with minimum ripple.

3. SRM Simulation by using FE Method

Because the magnetic field of SRM varies with rotor position. In the analysis of electromagnetic field following assumptions are presented.

(a) The end-winding magnetic field effects of the SRM are neglected. The magnetic field distributes invariable along the longitudinal axis. The magnetic vector potential A and the current density J only have the axial components A_z and J_z. The magnetic induction intensity only has the component B_x and component B_y.

(b) The material of the stator core is isotropic, and has single-valued B-H cure.

(c) Magnetic field outside the motor is neglected. The outer diameter circle of the stator and the internal diameter circle of the rotor are zero-vector magnetic line.

On the basis of above assumption, boundary value problem about calculation of two-dimensional electrostatic field can be expressed as the following [17]

$$\begin{cases} \dfrac{\partial}{\partial x}(\dfrac{1}{\mu}(\dfrac{\partial A_z}{\partial x}) + \dfrac{\partial}{\partial y}(\dfrac{1}{\mu}(\dfrac{\partial A_z}{\partial y}) = -J_z \\ A_z|_{\Gamma_1 \Gamma_2} = 0 \end{cases} \qquad (13)$$

where μ is the permeability of the material. Γ_1 is the outer diameter circle of the stator of the SRM. Γ_2 is the internal diameter circle of the rotor of the SRM. Then the calculation model for two dimension field numerical analysis is established.

Table I shows dimensions of a three phase 6/4 SRM that has been used. Both the permeability of the air and the winding are 1. The material of stator and rotor laminating is 0.5mm defined by using BH magnetizing curve have been showed in Fig. 2. A finite element analysis software, ANSYS, has been used to simulate a nonlinear magnetic 2-D model of this SRM for each solution produced by the GA.

Table I. Dimensions and Material Data of the Original Motor

Number of stator poles	6
Number of rotor poles	4
Stator outer diameter	12.4 cm
Air gap length	0.04 cm
Stator inner diameter	7.16 cm
Number of turns/phase	180
Stator pole height	1.62 cm
Stator pole arc	40 degree
Stator back iron thickness	1 cm
Rotor pole arc	42 degree
Rotor outer diameter	7.12 cm
Rotor pole height	2.1 cm
Stator and rotor core material	DBII steel
Stack depth	3.74 cm

Fig. 3: Design of rotor having arcuate teeth.

Fig. 4: Flux density profiles for different radius of arcuate rotor teeth.

Fig. 2: BH magnetizing curve of stator and rotor laminating.

Fig. 5: Inductance profiles for different radius of arcuate rotor teeth.

4. New Design of SRM

To decrease the acoustic noise in SRM, arcs on the rotor and stator teeth are designed in three steps.

a) Rotor with arcuate teeth

Arcs are designed only on the rotor teeth (Fig. 3). The radius of arcs can vary from ∞ (straight line) to half of the rotor pole height (half circle), $R_r \geq 1.05cm$.

To have more perception about the effect of curving rotor and stator on the SRM characteristics, three sets of ANSYS based simulations are performed. In the first simulation set, the stator is not arcuate and the rotor has arc values equal to ∞, 3, 2, and 1.5 cm. The corresponding simulation results are illustrated in figures 4-7. Figures 4, 5, 6, and 7 show the flux density, inductance, torque, and radial force of the SRM, respectively where phase current is equal to 2A. Figure 4 shows decreasing the radius of arcuate rotor increases flux density. As shown in figure 5, the incremental inductance decreases by reduction of the radius of arcuate rotor. Figure 6 shows that the torque increases in unaligned positions and decreases in aligned positions. Finally, figure 7 illustrates that decreasing the radius of arcuate rotor reduces radial force and as a result, the sound power decreases.
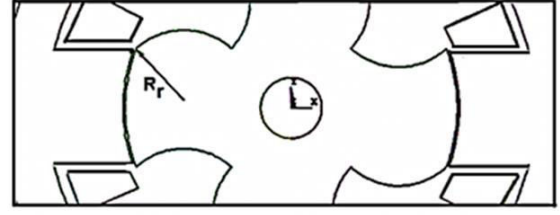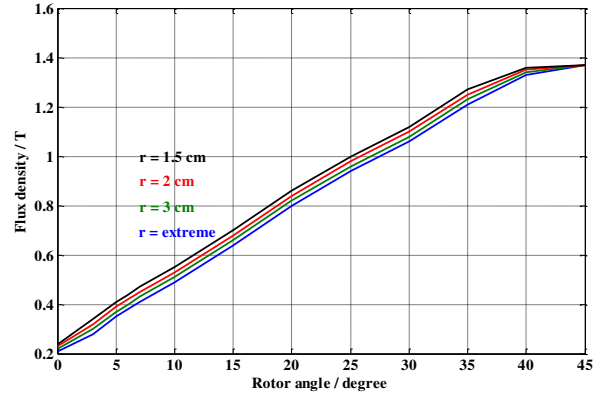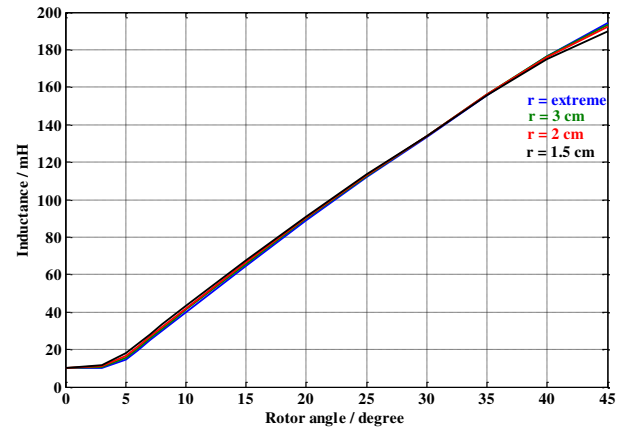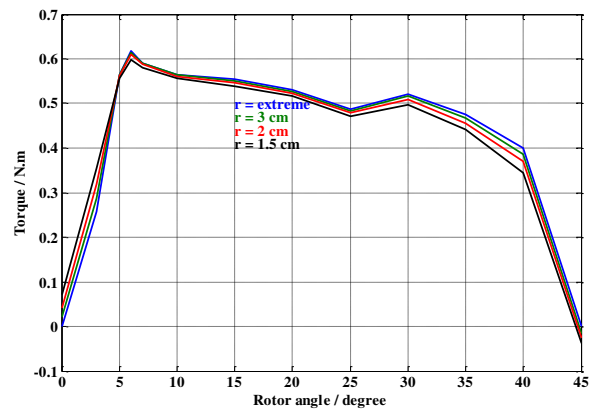

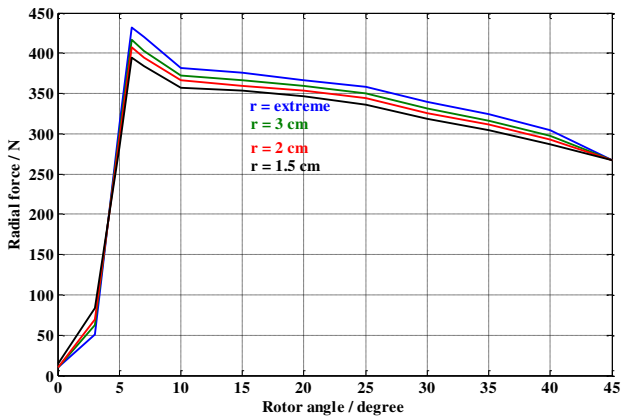Fig. 6: Static torque profiles for different radius of arcuate rotor teeth.

Fig. 7: Radial Force profiles for different radius of arcuate rotor teeth.

b) Stator with arcuate teeth

In the second step, arcs on the stator teeth are designed (Fig. 8). The radius of arcs can vary from ∞ (straight line) to half of the stator pole height (half circle), $R_S \geq 0.81 cm$. In the second simulation set, the rotor is not arcuate and the stator has arc values equal to ∞, 3, 2, and 1.5 cm. The corresponding simulation results are given in figures 9-12.

Figures 9, 10, 11, and, 12 show the flux density, inductance, torque, and the radial force of the SRM, respectively. Figure 9 shows decreasing the radius of arcuate stator increases the flux density in aligned positions. As shown in figure 10, the inductance is not varied by reduction of the radius of the arcuate stator. Figure 11 shows that the average torque is nearly constant. Finally, figure 12 illustrates that decreasing the radius of arcuate stator reduces the amplitude of radial force and as a result, the sound power decreases.
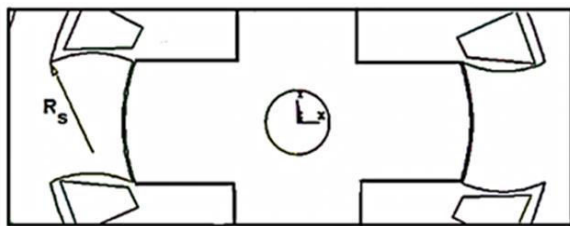

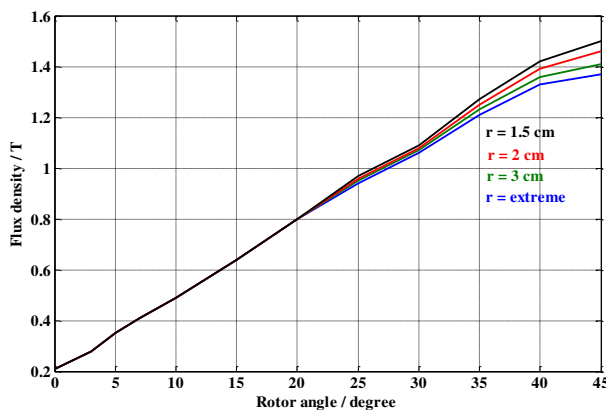Fig. 8: Design of stator having arcuate teeth.

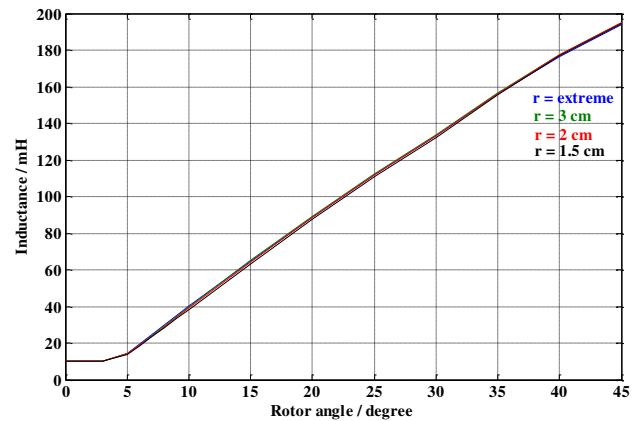Fig. 9: Flux density profiles for different radius of arcuate stator teeth.

Fig. 10: Inductance profiles for different radius of arcuate stator teeth.
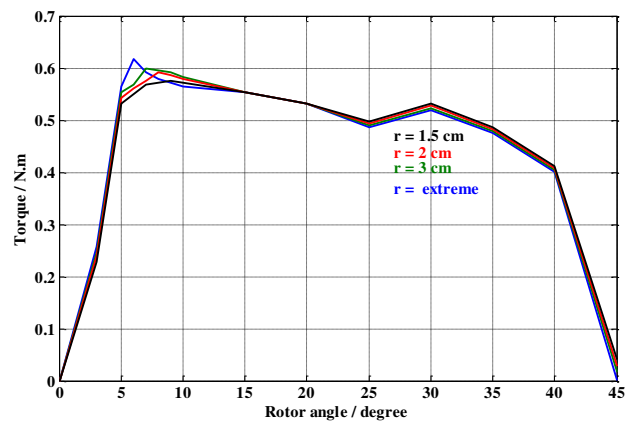

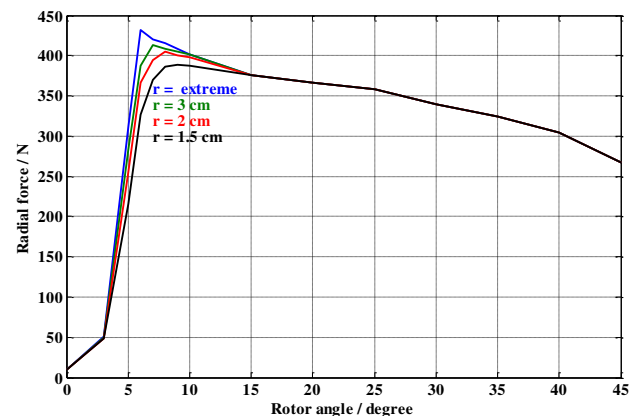Fig. 11: Static Torque profiles for different radius of arcuate stator teeth.

Fig. 12: Radial Force profiles for different radius of arcuate stator teeth.

c) Stator and Rotor with arcuate teeth

In the third step, arcs on the stator and rotor teeth are designed (Fig. 13). The radius of rotor and stator arcs can vary from ∞ (straight line) to half of the rotor pole height and half of the stator pole height (half circle), respectively ($R_r \geq 1.05 cm$ and $R_S \geq 0.81 cm$). In the third simulation set, both rotor and stator are arcuate and have the same arc values equal to ∞, 3, 2, and 1.5 cm. The corresponding simulation results are given in figures 14-17.
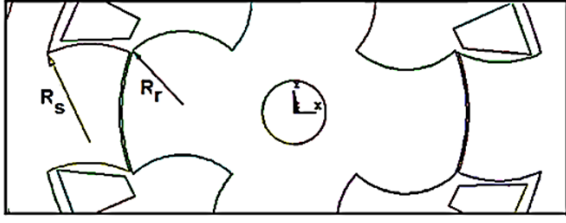
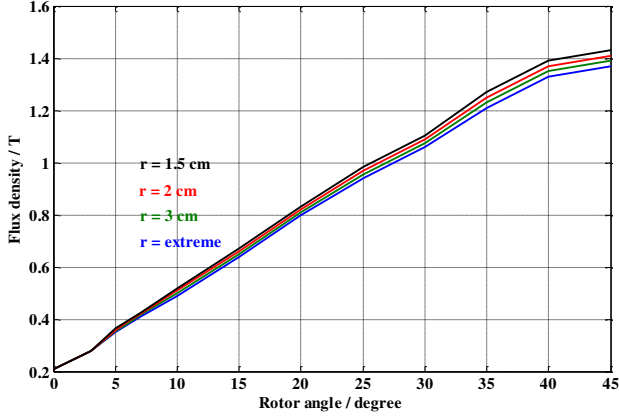Fig. 13: Design of Rotor and stator having arcuate teeth.

Fig 14: Flux density profiles for different radius of arcuate stator and rotor teeth.
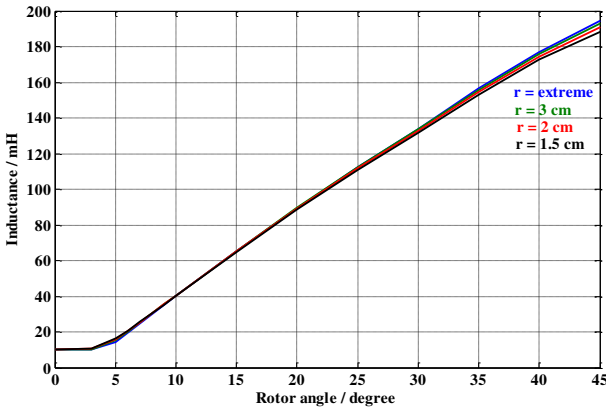

Fig. 15: Inductance profiles for different radius of arcuate stator and rotor teeth.
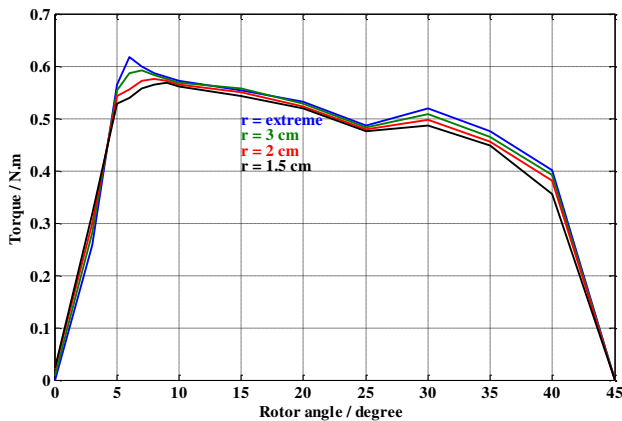

Fig. 16: Static Torque profiles for different radius of arcuate stator and rotor teeth.
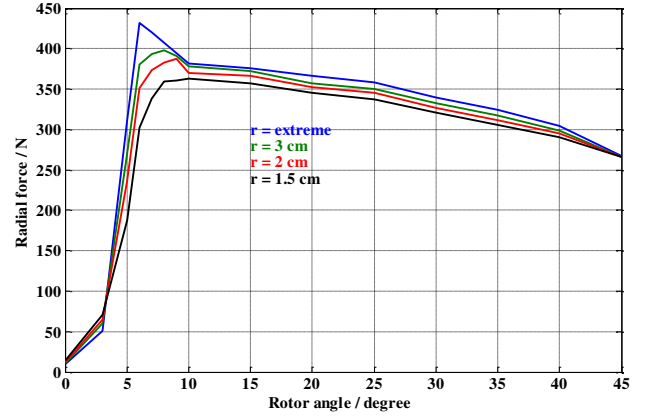

Fig. 17: Radial Force profiles for different radius of arcuate stator and rotor teeth.

Figures 14, 15, 16, and 17 show the flux density, inductance, torque, and radial force of the SRM, respectively. Figure 14 shows decreasing the radius of arcuate rotor increases flux density. As shown in figure 15, the inductance is nearly constant in unaligned positions and decreased in aligned positions by reduction of the radius of arcuate rotor. Figure 16 shows that the average torque decreases. Finally, figure 17 illustrates that decreasing the radius of arcuate rotor reduces the amplitude of radial force and as a result, the sound power decreases.

5. The Optimal Design of Stator and Rotor Pole

In these designs when the shape of poles varies, the mass of motors remains constant. Sound power radiated is lowest when the radial force and torque ripple are minimized. It is important to note that when the shape of poles varies during noise emission decrease, torque should not be decreased. Since, the sound power radiated is proportional with square of amplitude of radial force, the objective function for SRM sound power radiated is defined as:

$$F_{obj} = \frac{F_r^2 \times Ripple_T}{T_{av}} \qquad (18)$$

The minimum noise and maximum torque will occur when the objective function is minimized.

As discussed before, one phase of a 6/4 SRM is selected equal to 30° in which the torque is nearly constant. The whole rotor angle is 45 degrees. Hence, the interval of a phase would be [0º-30º] to [15º-45º].

Therefore, we face to multivariable problem which must be optimized. To solve this problem, the genetic algorithm is used. The GA have to found the optimum arc values for both stator and rotor and also the best phase interval so that the average torque does not reduce and the objective function, F_{obj}, would be minimized. The *optimtool* of MATLAB was used to implement our GA

optimization. Because of the type of our optimization problem variables, the population type of the GA was selected as *double vector*. The reason is that the rotor and stator arcs may have very large values. The population size was selected equal to 12 from which two best children are remained for the next generation. 60% of the rest populations are generated from crossover and the rest 40% from mutations. To have the lowest risk of holding in local minima, the mutation should be significant. Hence, a uniform mutation function with the rate of 0.3 was selected. Also, the scattered crossover function was chosen to generate children from parents. By using this setting of GA parameters, the algorithm reached to the best solution after only 38 epochs. Figure 18 shows the best and mean fitness function value (F_{obj}) for 100 epochs.

The best arc values for stator and rotor were obtained equal to 1.41cm and ∞, respectively. In other words, the best result occurs if only the stator is arcuate. In the GA optimization procedure, the arc values greater than 20cm are considered as ∞. Also, the optimum interval was obtained between 4.85° and 34.85°.

A comparison between the conventional and the optimized motors is given in table II. As shown in this table, the average torque values for both motors are approximately equal. The optimized motor causes only about 60% and 87.5% of the torque ripple and radial force of the conventional motor, respectively. Consequently, the fitness value of the optimized motor is about 45% of the fitness of the conventional motor. It demonstrates that the sound noise of the motor with the arcuate stator is much lower than the conventional motor, while their average torques are equal.
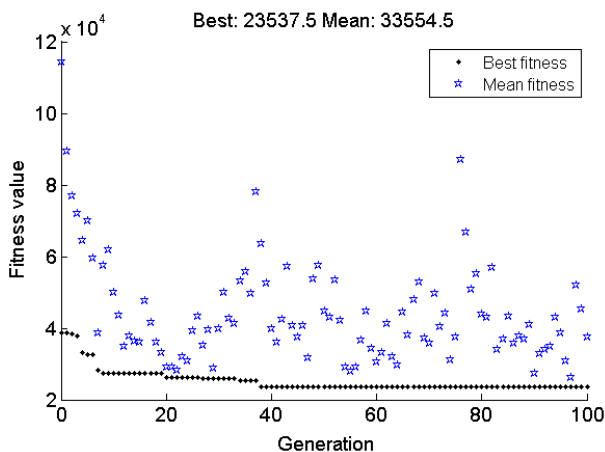
6. Experimental System

The specification of experimental model of SR motor was 2 A, 220-V, 1-hp, 6/4. The rotor was manufactured by steel layer having arcuate poles so that rotor dimensions are equal to the base rotor. This rotor has four poles, and its pole arcs are 2 degree greater than stator pole arcs. The arcuate rotor was assembled in the stator instead of the base rotor. Figure 19 shows the SR motor with a rotor having arcuate teeth. Figure 20 shows the base rotor of the SRM prototype. Figure 21 shows the drive of SR motor. After running the motor, the sound noise was measured by sound level meter. Comparison between the noises of the base motor and the motor with the arcuate rotor showed that the sound noise decreased when the rotor has arcuate poles.

7. Conclusion

In this paper, an optimum design of SRM for sound noise reduction is presented based on the genetic algorithm. The best GA solution determined that a motor the straight rotor and the arcuate stator with the arc value equal to 1.41cm . Also, the optimum interval was obtained between 4.85 and 34.85 degrees. By using the GA optimization procedure, the minimum fitness function obtained about 45% of the conventional motor after 38 generations. Experiments on a real arcuate stator motor validate the obtained optimum results. The real arcuate stator motor has much lower sound noise with about equal average torque than the conventional motor.

Fig. 18: The best and mean fitness function values (F_{obj}) obtained in each generation of the genetic algorithm

Table II: Comparison between the conventional and the optimized motors

	T_{av}	$Ripple_T$	F_r	F_{obj}
$R_r = R_s = \infty$	0.5318	0.1484	432	52186
$R_r = \infty$, $R_s = 1.41cm$	0.5312	0.0884	378	23537.5

Fig. 19: A SR motor containing a rotor having arcuate teeth.
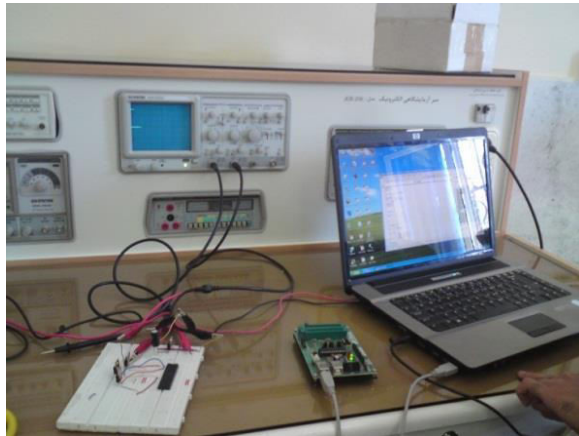

Fig. 20: Manufactured base rotor.

Fig. 21: Single-switch per-phase SRM converter.

References

[1] F. C. Lin, and S. M. Yang, " An approach to producing controlled radial force in a switched reluctance motor," *IEEE Trans. Industry Applications*, vol. 54, No. 4, pp. 2137 – 2146, August 2007

[2] D. E. Cameron, J. H. Lang , and S. D. Umans , " The origin and reduction of acoustic noise in doubly salient variable-reluctance motors," *IEEE Trans. Industry Applications*, vol. 28, No. 6, pp.1250 – 1255, 1992.

[3] Y.Ohdachi, Y. Kawase, Y. Miura, and Y. Hayashi, "Optimum design of switched reluctance motors using dynamic finite element analysis," *IEEE Trans. on magnetics*, vol. 33, No. 2, pp. 2033 – 2036, March 1997

[4] Y.Ozoglu , M.Garip, and E.Mese, "New pole tip shapes mitigating torque ripple in short pitched and fully pitched switched reluctance motors," *Industry Applications Conference, 2002. 37th IAS*, vol.1, pp. 43 – 50, 2002

[5] C.G.C. Neves, R.Carlson, N.Sadowski, , J.P.A.Bastos, and S.L.Nau, "The influence prediction of the current waveforms on the vibrational behavior of switched reluctance motors," *Electric Machines and Drives Conference Record, IEEE International*, pp. TB1-7.1-TB1-7.3, 1997

[6] F.Sahin, H.B.Ertan, and K.Leblebicioglu, "Optimum geometry for torque ripple minimization of switched reluctance motors," *IEEE Trans. on Energy Conversion*, vol. 15, No. 1, pp.31-39, March 2000

[7] N.K.Sheth, , and K.R.Rajagopal, "Optimum pole arcs for a switched reluctance motor for higher torque with reduced ripple," *IEEE Trans. on magnetics*, vol. 39, No. 5, pp. 3214 - 3216, September 2003

[8] N.K.Sheth, , and K.R.Rajagopal, "Torque profiles of a switched reluctance motor having special pole face shapes and asymmetric stator poles," *IEEE Trans. on magnetics*, vol. 40, No. 4, pp. 2035 – 2037, July 2004

[9] J. W. Lee, H. S. Kim, B.I. Kwon, and B. T. Kim, "New rotor shape design for minimum torque ripple of SRM using FEM," *IEEE Trans. on magnetics*, vol. 40, No. 2, pp. 754 – 757, March 2004

[10] Y. K. Choi, H. S. Yoon, and C. S. Koh, "Pole-shape optimization of a switched-reluctance motor for torque ripple reduction," *IEEE Trans. on magnetics*, vol. 43, No. 4, pp. 1797 – 1800, April 2007

[11] J. P. Hong, K. H. Ha, and J.Lee , "Stator pole and yoke design for vibration reduction of switched reluctance motor," *IEEE Trans. on magnetics*, vol. 38, No. 2, pp. 929 – 932, March 2002

[12] R. Lateb, N. Takorabet, and F. Meibody-Tabar, "Effect of magnet segmentation on the cogging torque in surface-mounted permanent magnet motors," *IEEE Trans. on Magnetics*, vol. 42, no. 3, pp. 442-445, 2006.

[13] A. Rezazadeh, "Genetic Algorithm based Servo System Parameter Estimation during Transients" *Advances in Electrical and Computer Engineering (AECE)*, vol. 10, pp. 77-81, 2010.

[14] A. R. Rezazade, M. Lankarani, "Parameter Estimation Optimization Based on Genetic Algorithm Applied to DC Motor", *Proceedings of ICEE 2007 International Conference on Electrical Engineering*, Lahore, Pakistan, 11-12 April 2007.

[15] H. Tahersima, M. Kazemsaleh, M. Tahersima, N. Hamedi, "Optimization of Speed Control Algorithm to Achieve Minimum Torque Ripple for A Switched Reluctance Motor Drive Via Ga" *4th International Conference on Power Electronics Systems and Applications (PESA)*, pp. 1-7, 2011.

[16] M.N.Anwar, and I.Husain, "Radial force calculation and acoustic noise prediction in switch reluctance machines," *IEEE Trans. on Industry Application*, vol. 36, No. 6, pp. 1589-1597, November/December 2000

[17] Li Weili, Sheng Man, Huo Fei "Optimal design and Finite Element Analysis of Switched Reluctance Motor for Electric Vehicles" *Vehicle Power and Propulsion Conference, 2008. VPPC '08. IEEE*